

NASA
1992
64

Preliminary Structural Design of a Lunar Transfer Vehicle Aerobrake

by

Lance B. Bush
B.S. August, 1985, Pennsylvania State University

A Thesis Submitted to the Faculty of Old Dominion University in
Partial Fulfillment of the Requirements for the Degree of

Master of Science

Engineering Mechanics

Old Dominion University

February, 1992

Approved by:

R. Prabhakaran
Dr. R. Prabhakaran (Co-Advisor)

Resit Unal
Dr. Resit Unal (Co-Advisor)

Gene Hou
Dr. Gene J. W. Hou

Larry Rowell
Larry Rowell

Acknowledgements

I would like to express my appreciation to Dr. Prabhakaran, my co-advisor, for his understanding and intuition in guiding me through my masters degree. The lessons learned in his classes were of essential value to my thesis and my technical development. I would like to give sincere thanks to Resit Unal, also my co-advisor. Resit's introduction of the Taguchi method to me was the key to this puzzle called a thesis. He has taught me much about design and in the process we have developed a friendship. Dr. Gene Hou's experience in optimization was of great help. His comments and suggestions helped to strengthen the technical content of the paper. Many thanks go to Larry Rowell, my assistant branch head and friend. Larry was unselfish with his time in helping me complete this thesis. His advice was invaluable, for the development of this thesis and myself.

Without the aide of Joe Rehder and Chris Cruz I could not have completed this study. Joe and Chris performed the vehicle packaging and aerodynamic studies, respectively. As usual, it was my pleasure to work with such professionals. Anne Costa's assistance in preparing the figures and the format of the text was greatly appreciated.

I would like to give special thanks to my mom, dad and sister for their gentle encouragements, emotional support and willingness to listen to me babble over long distance. Thanks also to my "little brother", David McGinnis for giving me much needed mental therapy in the forms of

basketball and video games. And to Shelley, I extend my deepest love and gratitude for all her loving support.

Thanks also to Kara, you are always with me.

Abstract

An aerobrake concept for a Lunar transfer vehicle was weight optimized through the use of the Taguchi design method, structural finite element analyses and structural sizing routines. Six design parameters were chosen to represent the aerobrake structural configuration. The design parameters included honeycomb core thickness, diameter-to-depth ratio, shape, material, number of concentric ring frames, and number of radial frames. Each parameter was assigned three levels. The minimum weight aerobrake configuration resulting from the study was approximately half the weight of the average of all twenty seven experimental configurations. The parameters having the most significant impact on the aerobrake structural weight were identified.

Table of Contents

	PAGE
List of Figures.....	v
List of Tables.....	vi
Nomenclature.....	vii
Symbols.....	vii
Acronyms.....	viii
Chapters	
I. Introduction.....	1
II. Inputs and Assumptions.....	8
III. Design and Analysis Methodology.....	13
Design Methodology.....	13
Analysis Methodology.....	17
IV. Preliminary Results.....	30
V. Design Matrix.....	33
VI. Results.....	41
VII. Conclusions and Recommendations.....	51
List of References	53

List of Figures

FIGURE	PAGE
1. Apollo LTV configuration	2
2. Aerodynamic capture.....	3
3. Lunar transfer vehicle configurations.....	5
4. Aerobrake heating for lunar return	11
5. Temperature performance of materials.....	12
6. L ₉ (3 ⁴) orthogonal array.....	14
7. EZDESIT finite element sizing methodology	20
8. Roarke table	24
9. Global buckling as a function of honeycomb core thickness.....	31
10. Concentric ring frames, radial frames and honeycomb core thickness.....	32
11. Ellipsoidal aerobrakes	35
12. Sphere/cone aerobrakes	36
13. Spherical aerobrakes.....	37
14. Response graphs.....	45
15. Interaction response graphs	46
16. Weight sensitivity of honeycomb thickness	49
17. Global buckling sensitivity of honeycomb thickness.....	49

List of Tables

TABLE		PAGE
I.	L27 Taguchi matrix.....	39
II.	Experiment matrix	40
III.	Experiment matrix with results	42
IV.	Response table	43
V.	Optimum configuration levels	48
VI.	Honeycomb thickness optimization	50

Nomenclature

Symbols

a	plate dimension, in.
A	cross sectional area, in. ²
Al	aluminum-2219
Al-Li	aluminum-lithium
b	plate dimension, in.
C-C	carbon-carbon
d	offset distance to centroidal axis, in.
E	Young's modulus, psi
g	gravitational constant, 32.2 ft/sec ²
h	honeycomb core thickness, in.
I	moment of inertia, in. ⁴
I _{offset}	offset moment of inertia, in. ⁴
I _{pre}	prescribed moment of inertia, in. ⁴
K	Rourke constant (fig. 9)
[K]	stiffness matrix
[Kg]	geometric stiffness matrix
L	unit length, in.
L/D	lift to drag ratio
L ₁₈	Taguchi matrix (18 experiments)
L ₂₇	Taguchi matrix (27 experiments)
L ₆₄	Taguchi matrix (64 experiments)

Symbols

N_{cr}	critical compressive load, lb/in.
N_{xcr}	critical compressive load (x-direction), lb/in.
N_{xycr}	critical compressive load (shear), lb/in.
N_{ycr}	critical compressive load (y-direction), lb/in.
N_{zcr}	critical compressive load (z-direction), lb/in.
t	flat plate thickness, in.
\bar{t}	average honeycomb sandwich thickness, in.
t_f	honeycomb facesheet thickness, in.
t_{min}	minimum facesheet gage, in.
w	weight of panel, lb
$\{\delta\}$	displacement vector
Δv	change in velocity
λ	eigenvalue
v	physical density of honeycomb core
ρ_c	material density of honeycomb core, lb/in. ³
ρ_f	material density of facesheet, lb/in. ³
σ_{xcr}	critical compressive stress (x-direction)

Acronyms

APAS	Aerodynamic Preliminary Analysis System
EAL	Engineering Analysis Language
EZDESIT	Finite element sizing routine
FEA	Finite Element Analysis
LTV	Lunar Transfer Vehicle
NASA	National Aeronautics and Space Administration
PATRAN	finite element modeling package

Acronyms

POST	Program to Optimize Simulated Trajectories
SEI	Space Exploration Initiative
SMART	Solid Modeling Aerospace Research Tool
TPS	Thermal Protection System

Chapter I - Introduction

A lunar colony is one mission among many being studied as part of the Space Exploration Initiative (SEI).^[1] The transportation of materials and personnel from Earth to the moon in support of a lunar colony constitutes a major technical challenge if the cost to deliver these payloads will not be exorbitant. A method of reducing the overall transportation costs is through the use of an efficient, space-based, reusable lunar transfer vehicle (LTV). The first LTV's were those of the Apollo missions (Fig. 1). The Apollo LTV's were ground-based. For many mission scenarios currently under consideration, LTVs supporting the lunar colony would be space-based, thus eliminating LTV launch costs into low-earth orbit for each mission. A space-based, reusable LTV would reside at the Space Station Freedom or a space platform and transfer payloads from its docking residence to the Moon and return.

The lunar missions involve large ΔV 's (changes in velocity) in order to transfer from the lunar return interplanetary transfer orbit to the Earth parking orbit (Fig. 2).^[2] These types of maneuvers are referred to as orbit capture. There are two primary methods to achieve capture. The current capture method is through the use of propulsion and has been used for all of NASA's planetary missions to date. To attain the necessary ΔV 's for orbit capture upon Earth return, a large amount of propellant would be needed and must be carried round trip to the Moon and return.

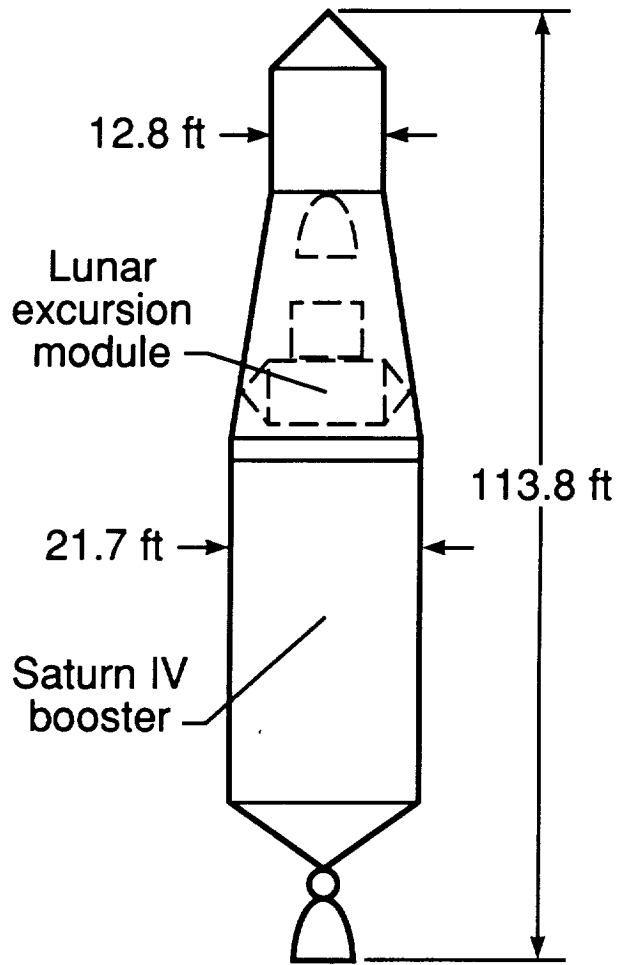


Figure 1. Apollo LTV.

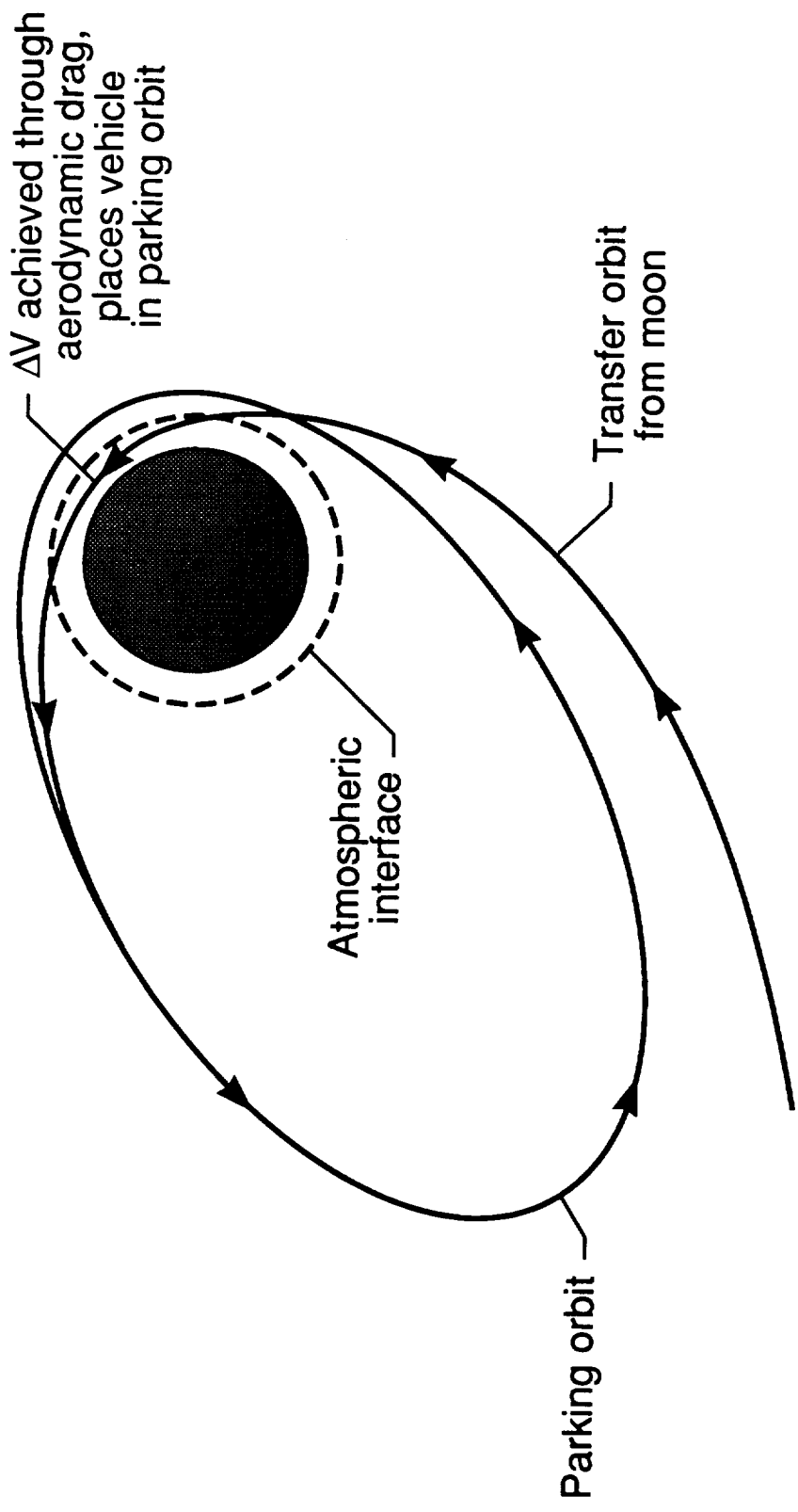
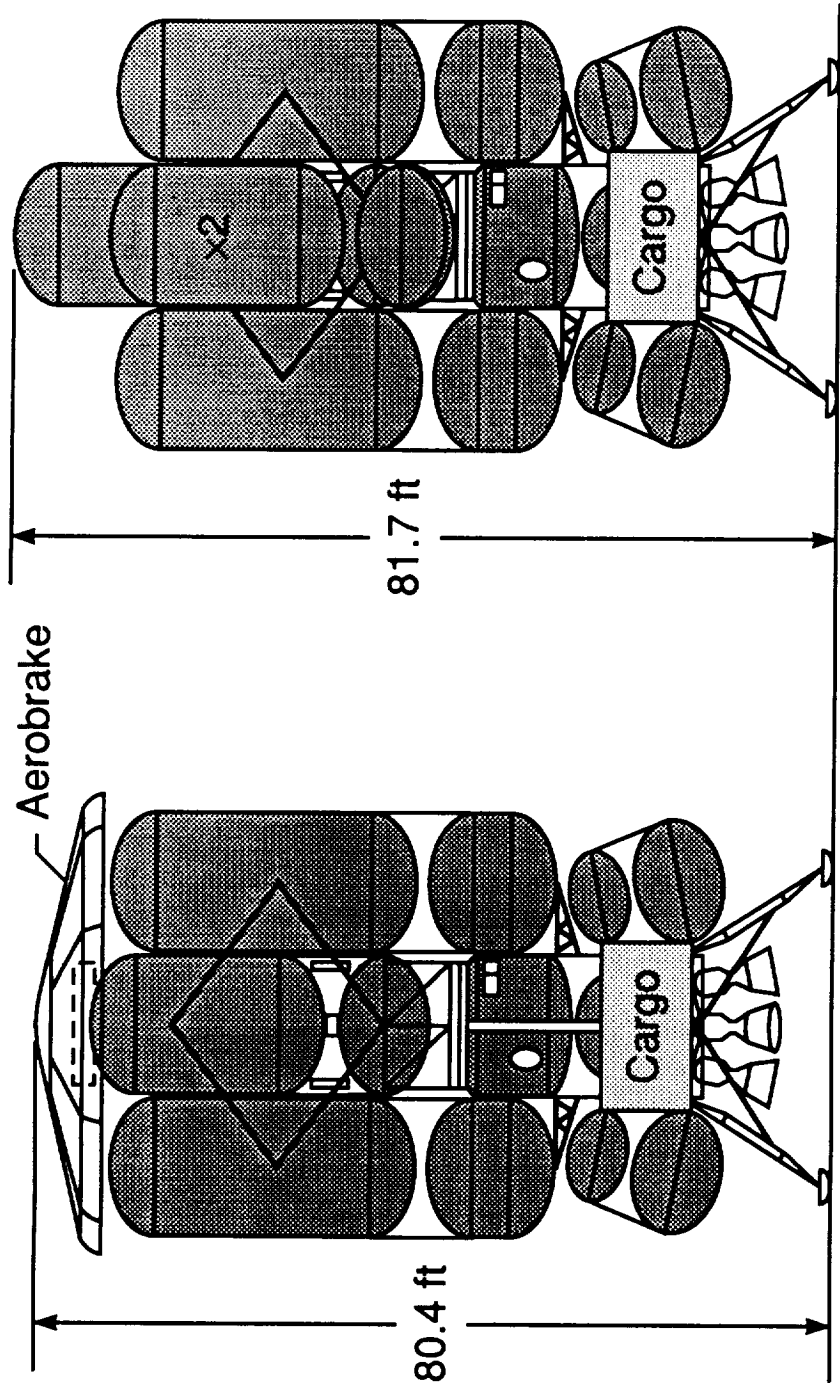


Figure 2. Aerodynamic capture.

An aerobrake (Fig. 3) offers an alternative, by attaining the necessary ΔV through a "passive" approach, eliminating the need for a propulsive capture burn at Earth perigee. An aerobrake grazes the atmosphere at Earth (Fig. 2), and thus utilizes drag to decrease velocity for capture. In general, aerobrakes are curved surfaces large enough to protect the spacecraft from hot gases in the wake and shaped so as to provide necessary lift, drag, and controllability. The concave side of the aerobrake is fitted with the spacecraft and the convex side is the aerodynamic surface, acting to slow the vehicle upon entry to the atmosphere.

A significant portion of all LTV's are made up of propellants and tanks (Fig. 3).[3] By utilizing an aerobraking device instead of a propulsive burn for capture, a significant amount of these propellants can be saved. Figure 3 shows the difference in size and tankage between a LTV with and without an aerobrake. In figure 3b the aerobrake is replaced with a significant amount of propellants and the size of the LTV has increased. Studies show a mass savings of 26 percent of the LTV gross weight to deliver a 15 ton lunar payload when substituting an aerobrake configuration for an all propulsive configuration.[4] Therefore, one Earth-to-orbit flight (109 tons payload) could be saved for each lunar mission. Thus, if an aerobrake could be used to passively achieve the necessary ΔV 's, a significant mass savings and associated costs may be realized. An aerobrake can be considered advantageous from a performance standpoint if the aerobrake mass is less than the propellant and propulsion system mass savings. In general, an aerobraked LTV appears to be advantageous only if the mass of the brake is less than 15 percent of the overall return mass of the vehicle.[5] Thus, the structural concept, material selection, and other design features must be



(a) LTV with aerobrake
 (b) All-propulsive LTV

Figure 3. Lunar Transfer Vehicle configurations (reference 4).

optimized in some fashion to produce the lowest weight aerobrake meeting performance requirements.

This study was initiated to identify a minimum weight lunar aerobrake structural design and the associated design parameter sensitivities based on fully stressed structural analysis techniques using a Taguchi design methodology. This study focuses on the aerobrake structural design, although the aerobrake design is dependent upon analyses from other disciplines such as aerodynamics, performance, weight, packaging, and heating. Some of the results from these areas leading to the concepts treated in this paper are reported in references 5,11, and 12.

Because of the broad range of design variables to be studied, the Taguchi methodology was applied to provide a systematic method for selecting combinations of variables for analysis. Typically in the past, the structural configurations selected for analysis were defined by the experience and engineering judgement of the designer. Within the time constraints of the study, simple, one parameter trades would be performed. These trades might alter the level of one parameter and analyze results while all other parameters were left constant. This approach has been necessary given the time constraints and the lack of strong physical definition of a concept at the time of conceptual/preliminary level design. However, this approach does not identify the possible interaction of the parameters or the combination of the parameter levels defining an optimum configuration. A full factorial approach, where every combination of all parameters are analyzed, could find the optimum configuration, but would be too time consuming.

For this study, the utilization of the Taguchi method was proposed to address this problem. The Taguchi method employs the use of orthogonal arrays based on the design of experiments theory. The design of experiments theory was developed in Great Britain in the 1940's for the improvement of crop production.^[6] Taguchi institutionalized the approach by creating a handbook of standard orthogonal arrays.^[7] The Taguchi method was then utilized in Japan to revolutionize the consumer product market; specifically, electronics.^[8] This approach has been used in other industries, but has just recently been utilized for aerospace design.^[9] The two-fold objective of this study is to obtain a minimum weight aerobrake structural configuration and demonstrate the applicability of the Taguchi method for aerospace vehicle structural design. The results of this study have served to bolster the advocacy of the Taguchi method for aerospace vehicle design. Reduced analysis time and an optimized design both demonstrated the applicability of the Taguchi method to aerospace vehicle design.

Chapter II - Inputs and Assumptions

Prior to this structural design and analysis study, aerodynamic analyses and a packaging study were performed in order to establish performance requirements and determine viable shapes for an aerobrake similar to that in Fig. 3a. Hundreds of shapes were tested, including spheroids, ellipsoids, hyperboloids, and sphere/cone configurations, all with several levels of geometry parameters including effective nose radius, cone angle, diameter-to-depth ratio, etc. Packaging studies addressing fit within wake flow and center-of-gravity placement resulted in a baseline aerobrake diameter of 50 ft and a 40,000 lb cylindrical payload of 25 ft diameter. The aerodynamic analyses of the selected shapes were performed at flight conditions of Mach 20 and an altitude of 200,000 ft in order to match the flight entry corridor for aerobraking trajectories, that were constrained to an inertial loading of five g's acceleration.

The inertial and aerodynamic loads incurred during the mission are assumed to be critical. Ground operations, maintenance, handling, and transportation have yet to be defined for the aerobrake vehicle, and the loads incurred during manufacturing, transportation, and maintenance are reserved for further studies.

In order to perform a timely study, some basic initial assumptions were adopted. The surface panels of the aerobrake are a honeycomb sandwich

construction. A large, transversely loaded surface such as an aerobrake incurs large bending moments. Transverse structure thickness stiffens the structure, preventing bending. Honeycomb panels, isogrid panels, and a membrane skin with a complex truss structure arrangement are the best options for the aerobrake structure. Both isogrid panels and membrane skins with a complex truss structure must be designed for the loading conditions and geometric fit within the physical boundaries of the aerobrake. Isogrid panels or membrane skin with complex truss structure add complexity to the models, and thus, the honeycomb sandwich was selected for this conceptual/preliminary level assessment.

Stiffeners for the aerobrake include radial frames and concentric ring frames. Stiffener directions were selected to match the major load paths of the vehicle; hoop and radial.

The launch configuration of the aerobrake vehicle is dependent upon the packaging constraints of the Earth-to-orbit launch vehicle. Little definition of the on-orbit assembly method and mechanisms for aerobrakes exists. Thus, the baseline configuration was assumed to be an on-orbit bonded/welded structure.

The three materials selected for the aerobrake structure are aluminum-2219 (Al), aluminum-lithium (Al-Li) and carbon-carbon (C-C). These three materials represent three different levels of technology, conventional, near-term, and advanced. Materials for aerobrakes must be capable of surviving the high temperature environments occurring during atmospheric reentry. Thermal analysis of a 45 ft. diameter sphere/cone aerobrake with a 10 ft.

nose cone radius and a 20° cone sweep angle implicate the need for materials to withstand temperatures of at least 3200° F (Fig. 4). The low thermal capability of aluminum and aluminum-lithium structures dictates a need for a thermal protection system (TPS) as shown in Fig. 5.[10] The additional weight of the TPS will be added to the final structural weight of the aluminum-based configurations so a fair comparison can be made with the weight of the carbon-carbon configuration which needs no additional TPS. The TPS selected must satisfy the on-orbit installation, repair, refurbishment, and inspection requirements; and thus, may not be the best insulating or lowest mass. Yet, because no specifications of these on-orbit requirements exist at present, the TPS will be chosen for analytical purposes on the basis of its thermal and mass characteristics. A survey of various TPS's including rigid and flexible and tile and ablators was performed.[11,12] The survey data indicates that an advanced carbon/carbon TPS with an average area mass density of 1.75 lb/ft² may be assumed to fulfill the temperature and thermal gradient considerations.

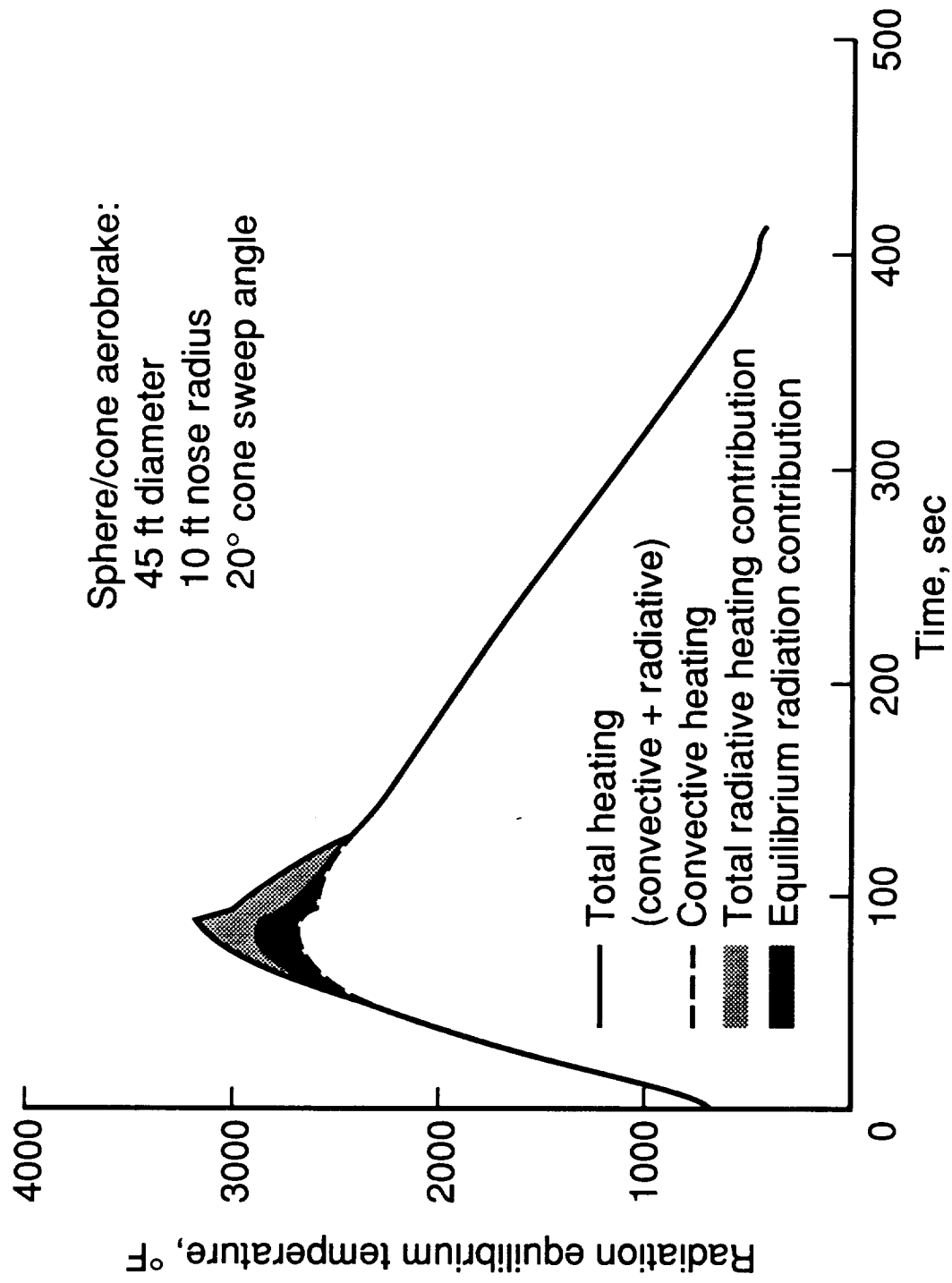


Figure 4. Aerobrake heating for lunar return.

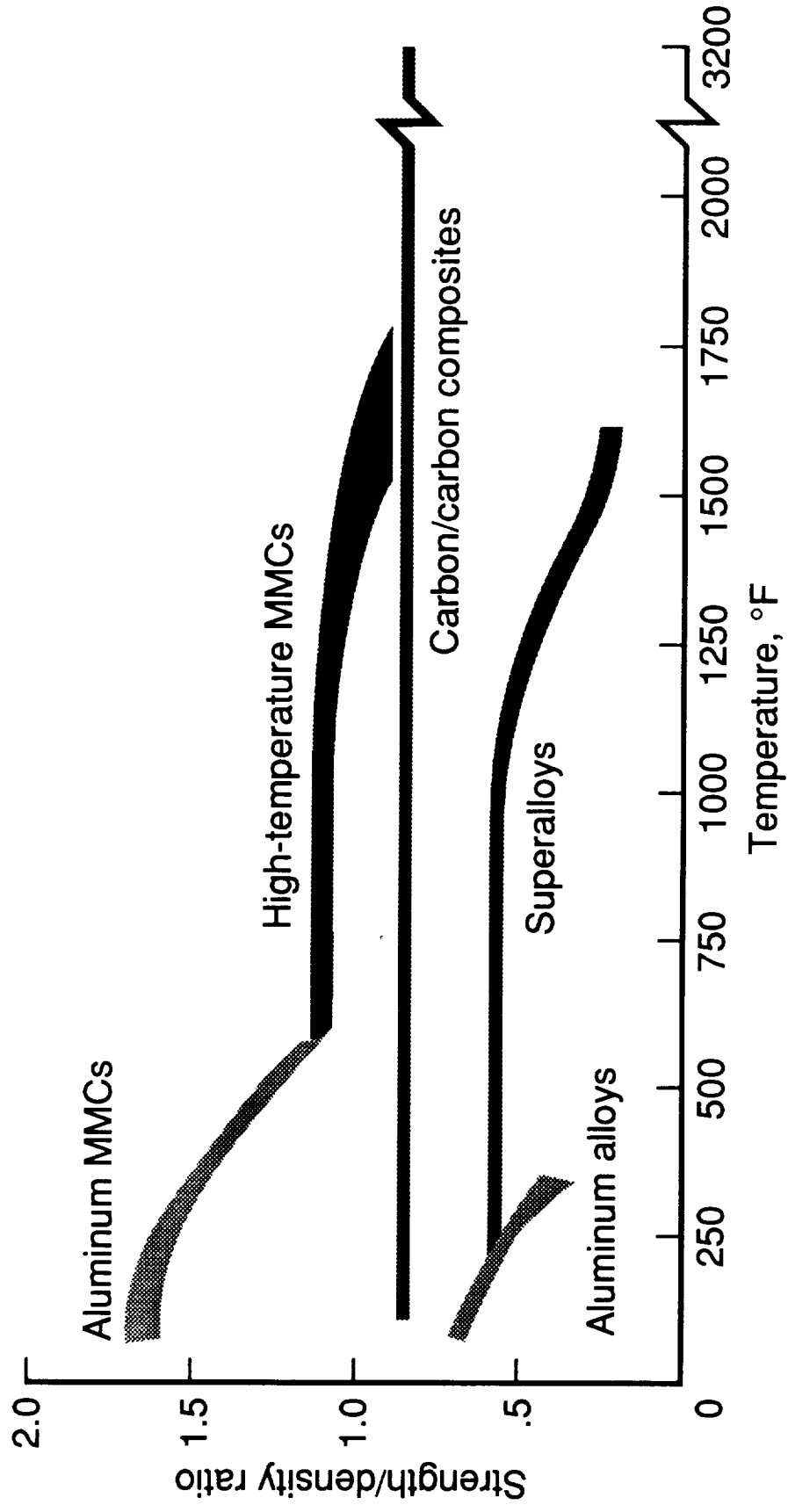


Figure 5. Temperature performance of materials.

Chapter III - Design and Analysis Methodology

Study Matrix

For the six design variables defined at three levels as previously mentioned, a full study matrix for all possible combinations would require 729 cases to be analyzed. A systematic approach to selecting an appropriate subset of these is needed.

The Taguchi method uses orthogonal arrays from design of experiments theory. Through the use of orthogonal arrays the number of experimental configurations to be studied is significantly reduced while providing essentially the same effective information as in a full factorial experiment. As a simple example, a array or matrix for 4 design variables each at 3 levels is shown in Fig. 6. In this array, the columns are mutually orthogonal. That is, for any pair of columns, all combinations of factor levels occur; and they occur an equal number of times. There are four factors (A, B, C, and D), each at three levels. This is called an L_9 design, where the 9 indicates the nine rows, or configurations to be tested, with test characteristics defined by the row of the table. The number of the column of an array represents the maximum number of factors that can be studied using that array. Note, that this array reduces 81 (3^4) configurations to 9. There are greater savings in testing for the larger matrices as is the case for this study. For example, a full factorial experimental design involving 10 parameters to be studied at three levels requires 59,049 experiments

	A	B	C	D
1	1	1	1	1
2	1	2	2	2
3	1	3	3	3
4	2	1	2	3
5	2	2	3	1
6	2	3	1	2
7	3	1	3	2
8	3	2	1	3
9	3	3	2	1

Figure 6. $L_9(3^4)$ orthogonal array.

(3¹⁰). Utilizing an orthogonal array can reduce the number of experimental configurations to 27.

The design methodology for this study using the Taguchi method employs seven basic steps:[13,14]

1. Identify the design parameters and their alternative levels,
2. Define possible interactions between these parameters,
3. Select an appropriate Taguchi orthogonal array,
4. Determine the parameter arrangement,
5. Conduct the matrix experiment using the finite element analysis,
6. Create response tables, graphs and analyze data,
7. Determine the optimum levels for the design parameters, and verify.

In step one, the design parameters and their corresponding levels are identified. Selection of the parameters and their levels determines the design space and must be done intelligently. The Taguchi method will determine the combination of the parameter levels that gives the optimum performance (i.e., low weight) and the sensitivity of the results.

In step two, the possible interactions between the design variables are selected for investigation based on experience. If interactions are not correctly identified at this stage, the results of the study will indicate so

with inconsistent data. If this occurs, the design process must be restarted with new interactions selected.

An appropriate Taguchi matrix is selected in step three. Standard Taguchi matrices exist in reference handbooks.[7] The selected matrix must be selected to accommodate the parameters, their levels, and the interactions. The matrix must contain at least one column for each parameter and each interaction. The number of levels will determine the number of rows in a matrix.

The fourth step of the procedure is to determine the parameter arrangement in the matrix. The arrangement is dependent upon the chosen parameter interactions. For more details on parameter arrangement refer to Ref. 15.

In step five the matrix experiments are conducted. The experimental method is dependent on the nature of each problem. For this study, the experimental procedure will be conducted by performing a finite element analysis of each experimental configuration. A finite element structural analysis of an aerobrake model yields an estimated physical representation of the effects of the external loading and its consequent resultant loads on the structure. This procedure is described in the analysis method section of this paper.

The results of the experiment are recorded and analyzed in step six. The result for each experiment is listed and an average value is calculated for each experiment having a specified parameter level. A comparison of the

average results for one level against that of the other levels within a parameter indicate the sensitivity due to that specific parameter. The difference between the greatest and least average value for each parameter gives an indication of the relative degree of sensitivity when compared with the difference for other parameters. For non-interacting parameters, the optimum level is identified by the lowest averaged result. Interacting parameter results are analyzed differently. All experiments having a particular level for one parameter and a particular level for another parameter are averaged. These values are placed in a matrix table. The optimum value within the table indicates the optimum levels for the two parameters.

In step seven, the optimum levels for the parameters are chosen and verification tests are run. Further experimentation can be attempted if the sensitivity graphs indicate any further optimization is possible outside the original design space.

Analysis Methodology

A finite element modeling and analysis technique is utilized to determine the integrity of each aerobrake structural arrangement. Of primary concern is the ability of each candidate structure to resist local mechanical failure modes and global buckling when subjected to aerodynamic and inertial loading present during the mission. Thus, each configuration analysis includes geometry modeling, finite element modeling, external load generation and application, finite element

analysis, structural element sizing, structural element weight summation, and post-processing results evaluation.

The geometry concepts are modeled through the use of the SMART (Solid Modeling Aerospace Research Tool) system.^[16] The models are stored as bicubic patch data, which is transferred to the finite element and aerodynamics packages.

Typically, the final external geometry of a candidate configuration is determined on the results of aerodynamic studies aimed at achieving necessary or optimum aerodynamic characteristics. The aerodynamic analysis is performed utilizing a modified Newtonian technique included in the APAS (Aerodynamic Preliminary Analysis System) code.^[17,18] Aerodynamic surface pressures are calculated and mapped from the aerodynamic model onto the structural finite element model.

The structural finite element model is derived by discretizing the SMART geometry surface into a finite element model. Internal structure and additional surface definition are created based on structural engineering experience. Internal structural arrangements may include ring frames, longerons, bulkheads, and truss structures. These structures are incorporated into the vehicle to withstand the external loading and provide safe loading paths, making the vehicle capable of completing the mission without structural failure. The desired material properties of the structure are also included in the finite element model of the vehicle.

As previously mentioned, the aerodynamic pressures resulting from the aerodynamic analysis are mapped from the aerodynamic grid to the structural grid. These aerodynamic loads along with the inertial loads calculated through a performance analysis combine to simulate the critical mission loading conditions. The inertial acceleration vectors are calculated utilizing POST (Program to Optimize Simulated Trajectories).[19] The finite element structural model is completed with the addition of the external loading and is ready for analysis.

Finite element analysis (FEA) is performed on the finite element model in order to determine the resulting loads due to the mission loading conditions. FEA is performed utilizing the Engineering Analysis Language (EAL).[20] The FEA produces resultant structural loads for each finite element. These resultant loads are indicative of the load paths and integrity of the vehicle structure and may indicate areas of the vehicle that are stressed beyond the limits of the construction material.

These loads are used as input to a structural sizing routine in order to determine the necessary increases in component size to meet failure criteria. Each structural element (bars, planar beams, and plate elements) is sized within the EZDESIT program to withstand the mission loading conditions (Fig. 7).[21] The cross-sectional areas of bar elements are sized. The cap cross-sectional areas and web height are sized for planar beams. The plate element design variables depend on the type of construction chosen. Isotropic and composite honeycomb, hat-stiffened, and membrane panels along with corrugated web elements can be sized by the EZDESIT code. For each element, a stiffness matrix and a construction geometry

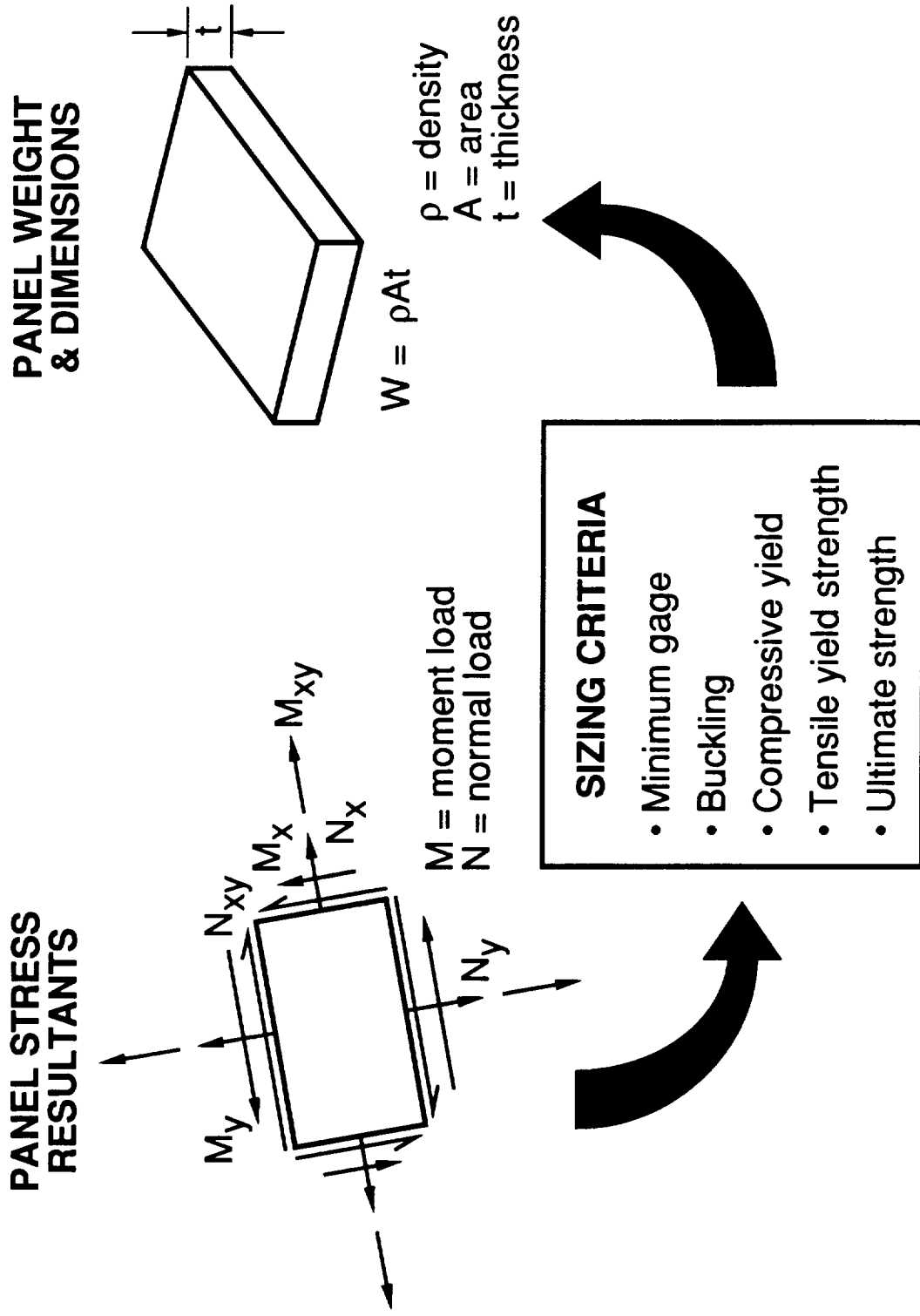


Figure 7. EZDESIT finite element sizing methodology.

(lamina gage, honeycomb core height, etc.) are specified, based on inputs such as minimum facesheet gage. The elements are sequentially checked for failure due to panel buckling, compressive yield, tensile yield, and ultimate strength failure modes for each loading case. If failure occurs, specific structural dimensions are increased until the particular failure mode is satisfied. The weight of each structural finite element is recalculated with each change of physical dimension. The weight of all the structural finite elements are added to obtain the structural weight of the aerobrake. The geometric sizing of the structural elements alters the stiffness properties of the aerobrake finite element model. Thus, the finite element analysis and structural element sizing are iterated until a aerobrake weight convergence is achieved. Convergence occurs when the difference between the structural weight of two consecutive iterations is negligible. A converged solution typically takes three iterations.

As an example of the sizing technique, the isotropic honeycomb sandwich structural sizing logic is explained here. Initial inputs to the structural sizing routine include the physical properties, such as honeycomb minimum and maximum thickness, minimum face gage thickness, and face sheet and honeycomb material properties. An average honeycomb sandwich thickness is calculated as:

$$\bar{t} = 2t_f + hv \quad (1)$$

where

t_f = one face sheet thickness

h = honeycomb thickness

v = physical density of honeycomb core (.02)

Next, a moment of inertia is calculated for the honeycomb panel.

$$I = I_{\text{offset}} + Ad^2 \quad (2)$$

where A = cross sectional area

$$I = t^3L/12 + 2(h/2)^2tL \quad (3)$$

where $L=1$ and $t^3/12 \ll (h/2)^2t$

$$\text{thus } I = h^2t^3/2 \quad (4)$$

Critical compressive stress for buckling in a flat plate is determined using a Rourke table^[22] (Fig. 8).

$$\sigma_{\text{xcr}} = K [E/(1-\nu^2)](t/b)^2 \quad (5)$$

The critical load (N_{xcr}) becomes;

$$N_{\text{xcr}} = K [E/(1-\nu^2)](t^3/b^2) \quad (6)$$

where E = Young's Modulus

a = plate dimension

b = plate dimension

$K = f(a/b)$

The conversion from a flat plate critical buckling failure load to a honeycomb sandwich critical buckling failure load is as follows.

$$t^3 = 12I/L \quad \text{for a flat plate} \quad (7)$$

$$N_{\text{xcr}} = 12KEI/[(1-\nu^2)(b^2)] \quad (8)$$

where $I = h^2t^3L/2$ for a honeycomb sandwich

After calculating the critical compressive load for the x, y and shear components (N_{xcr} , N_{ycr} , N_{xycr}), the buckling check is as follows.[23]

$$N_{cr} = N_x/N_{xcr} + N_y/N_{ycr} + (N_{xy}/N_{xycr})^2 \quad (9)$$

If $N_{cr} < 1$ Buckling does not occur

If $N_{cr} > 1$ Buckling occurs

If buckling occurs the honeycomb sandwich is sized to give the lightest weight honeycomb for its prescribed moment of inertia, subject to facesheet minimum gage and core height requirements. The sizing procedure follows. The prescribed moment of inertia is calculated as such:

$$I_{pre} = N_{cr}(I) \quad (10)$$

A facesheet thickness is derived from the prescribed moment of inertia and the current honeycomb height.

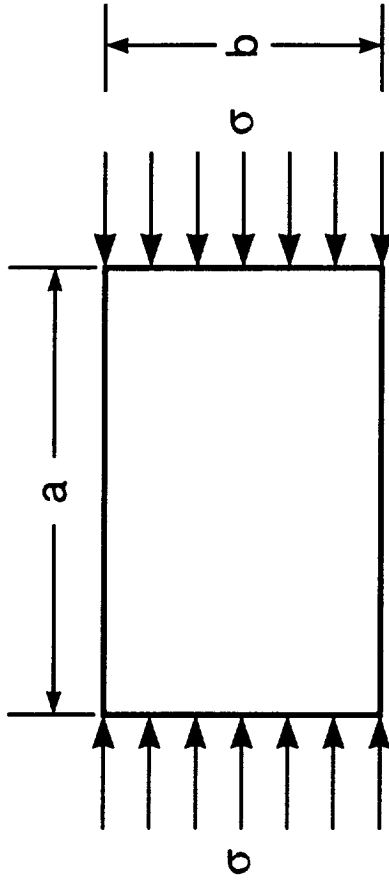
$$t_f = 2I_{pre}/h^2L \quad (11)$$

The weight of a unit length ($L=1$) of the sandwich honeycomb core is calculated as follows.

$$w = 2t_f\rho_f + v h\rho_c \quad (12)$$

where ρ_f = material density of the facesheet
 ρ_c = material density of honeycomb core

Formula for rectangular plate under equal uniform compression on two opposite edges b



$$\frac{b}{t} > 10$$

$$\sigma_{xcr} = K \frac{E}{1 - \nu^2} \left(\frac{t}{b} \right)^2$$

a/b	K
0.2	22.20
0.3	10.90
0.4	6.92
0.6	4.23
0.8	3.45
1.0	3.29
1.2	3.40
1.4	3.68
1.6	3.45
1.8	3.32
2.0	3.29
2.2	3.32
2.4	3.40
2.7	3.32
3.0	3.29
∞	3.29

Figure 8. Rourke table.

This weight is recorded and the honeycomb core height is step increased until it reaches the maximum core height. At each core height the facesheet thickness and corresponding structural finite element weight are recalculated. The honeycomb height and facesheet thickness that produce the minimum structural element weight of all the combinations are saved. The average honeycomb sandwich thickness (\bar{t}) is calculated and checked against the original value. If \bar{t} is greater than the original value, then the panel is considered to be panel buckling sensitive and the values for honeycomb core thickness, facesheet thickness, and \bar{t} are returned to the main program for the next test criteria, compressive yield at ultimate loads.

The compressive yield check begins by calculating the minimum facesheet gage based on in-plane mechanical loads. This gives a minimum facesheet gage value as a baseline for consequent tests. A Von Mises reduced allowable stress is calculated by subtracting the Von Mises stress due to thermal loads from the Von Mises allowable stress. A root bisection technique is employed to derive a facesheet thickness satisfying the Von Mises reduced allowable strength and the input loads. If this thickness is greater than the minimum facesheet thickness, then the new facesheet thickness replaces the minimum facesheet thickness for the structural element.

The honeycomb core thickness is sized to obtain the lightest weight facesheet thickness and honeycomb core thickness combination. A closed loop solution is utilized, subject to the following primary and secondary design equations and limit equations.

$$w = 2t_f\rho_f + v h\rho_c \quad \text{Primary Design Equation} \quad (13)$$

$$I = t_f h^2 / 2 \quad \text{Secondary Design Equation} \quad (14)$$

The limit equations are as follows.

$$t_{\min} < t$$

$$\text{minimum core height} \leq h \leq \text{maximum core height}$$

Combining the primary and secondary design equations yield the following.

$$w = 4I\rho_f/h^2 + v\rho_c L \quad (15)$$

The partial derivative of the structural element weight with respect to the honeycomb core height is taken as follows.

$$\partial w / \partial h = -8I\rho_f/h^3 + v\rho_c \quad (16)$$

An optimum structural element weight is found at an inflection point or when, the derivative is zero.

$$\partial w / \partial h = 0 \quad (17)$$

$$0 = -8I\rho_f/h^3 + v\rho_c \quad (18)$$

$$h = (8I\rho_f/v\rho_c)^{(1/3)} \quad (19)$$

Both the facesheet thickness and honeycomb core height are checked to make sure they satisfy the limit equations and are recalculated as needed based on the sizing logic.

Thus, a minimum facesheet thickness and honeycomb core height based respectively on in-plane mechanical loading and minimum moment of inertia to prevent buckling are derived as baseline values for a stepping optimization procedure. The lightest weight honeycomb facesheet thickness and honeycomb core thickness combination is searched for by stepping through the honeycomb core thickness values from the minimum core height to the maximum core height, while calculating the facesheet thickness at each step to satisfy the Von Mises allowable stress condition.

The compressive yield check is done for both the upper and lower surfaces of each panel to account for the change in sign of the loads in the panels. A maximum resulting honeycomb core height and facesheet gage height are selected from the upper and lower surface results. A new \bar{t} is calculated and checked against the previous value. If the new \bar{t} is greater than the previous value, the panel is considered to be compressive yield sensitive and the values for honeycomb core thickness, facesheet thickness, and \bar{t} are returned to the main program for the next test criteria, tensile yield.

The tensile yield check is performed by reducing the mechanical loads to the limit level and using the same methodology as that of the compressive yield. If the new \bar{t} is greater than the previous value, then the panel is considered to be tensile yield sensitive and the values for honeycomb core thickness, facesheet thickness, and \bar{t} are returned to the main program for the next test criteria, ultimate strength.

The ultimate strength check is performed by calculating the principle stress angles and transforming the thermal loads into a mechanical load state. These loads are used to reduce the principal allowables. The principal mechanical loads are then checked against these reduced

principal allowables. If the principal mechanical loads are greater than the reduced principal allowables, the skin thickness is increased by 10 percent. This continues until the principal mechanical loads are less than the principal reduced allowables. A new \bar{t} is calculated and checked against the previous value. If the new \bar{t} is greater than the previous value, then the panel is considered to be ultimate-strength-sensitive and the values for honeycomb core thickness, facesheet thickness, and \bar{t} are returned to the main program.

After all structural elements of the model have been sized accordingly, the finite element model is reanalyzed with the new stiffness. Following the analysis, the elements are resized for the new loads and this procedure continues until the overall vehicle model weight converges, usually about 3 iterations.

The results of the sizing can be reviewed in two different manners. An interactive session of the EZDESIT program permits the designer to review the data in tabular form. The structural weight of the aerobrake structure is calculated and displayed by component, load case, failure mode, and element type. In the second method, the EZDESIT results are read into PATRAN,^[24] a finite element pre- and post-processor, and the structural element results are displayed pictorially on the model. The results include resulting loads, dominant load case, failure modes, and unit weights. Highly loaded areas may indicate a need for an alternative structural design. If necessary, resultant loads are reviewed by the structural designer, and the necessary changes to the structural arrangement are made by altering the finite element model and reanalyzing the structure.

Each finite element model is checked for global buckling. The eigensolver routine of EAL is utilized to determine the percent of static loads

necessary to obtain a globally buckled model. An eigensolution is performed on the following equation.

$$[K]\{\delta\} - \lambda[Kg]\{\delta\} = 0 \quad (20)$$

K= stiffness matrix

Kg = geometric stiffness matrix

δ = displacements

λ = eigenvalue

When the eigenvalue is less than one, the loads are too great and global buckling occurs. Thus an optimum configuration would attain a global buckling eigenvalue of one plus additional margin for the factor of safety.

Chapter IV - Preliminary Results

A few aerobrake concepts were analyzed prior to establishing the design matrix in order to obtain a reasonable range of parameter values for testing. These preliminary results show the relationship between honeycomb thickness variation and global buckling to be sensitive (Fig. 9). This analysis was conducted for a 37.5 ft diameter aerobrake, with a diameter/depth of 1.5, and an ellipticity of 0.5. The aerobrake model assumed aluminum-2219 honeycomb with 4 concentric ring frames and 10 radial frames. According to Figure 9, a honeycomb thickness of at least 2.64 in is necessary to maintain structural integrity. Based on these results a minimum honeycomb thickness of 2.75 in was selected for the design matrix in an attempt to reduce the occurrence of global buckling. The preliminary results indicated that global buckling was the driving failure criteria over the localized phenomena such as yield and ultimate stresses. Thus, when defining the structural parameters, great attention was placed on attempting to alleviate the global buckling phenomena. The number of concentric ring frames and radial frames along with the honeycomb thickness (Fig. 10) have an effect on global buckling. Thus, these structural parameters were also chosen as design parameters. These three parameters along with the previously mentioned diameter-to-depth ratio, shape, and material make up the six design parameters for this study.

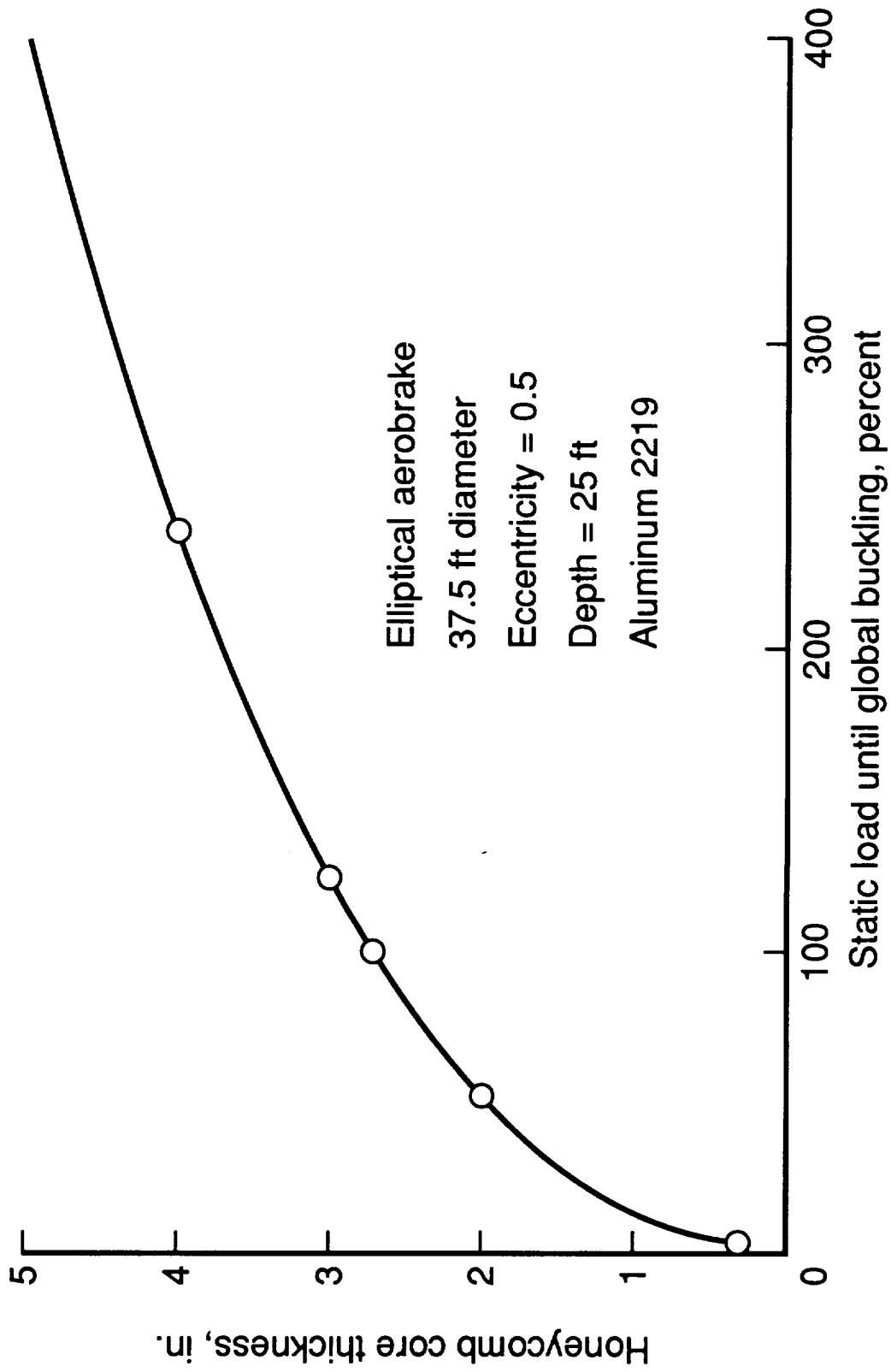


Figure 9. Global buckling as a function of honeycomb core thickness.

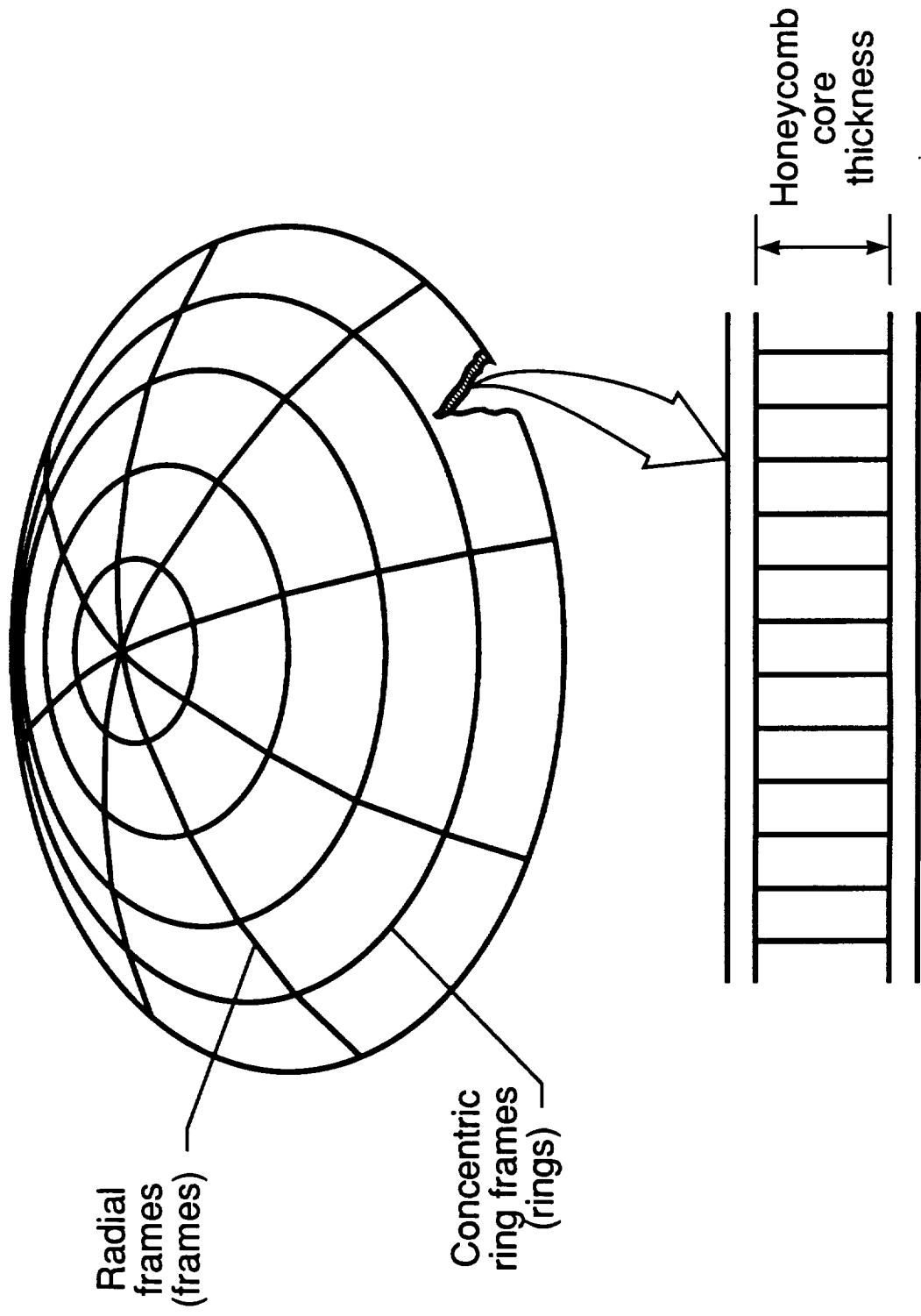


Figure 10. Concentric ring frames, radial frames, and honeycomb core thickness.

Chapter V - Design Matrix

A design space must be defined for the Taguchi optimization by defining the design parameters and their levels. The design parameters and their levels must be chosen based upon experience and knowledge as poor choices of levels will incur the need for further studies. For this study, aerodynamic, packaging, structural, and material concerns impacted the selection of the parameters and their levels. The decision process for the parameters follows.

As mentioned previously, hundreds of aerobrake shapes were aerodynamically analyzed. The number of candidate configurations was reduced on the basis of their packaging capabilities, with regards to the wake turning angle, and aerodynamic performance. Still, many candidate shapes remained viable. No further aerodynamic or performance criteria were applied to reduce the number of candidates. The selection from these viable candidates then was to be based on structural and weight considerations. Thus, the structural analysis was used as a design tool for the aerobrake selection. So many configurations remained that an orderly and efficient analysis method was necessary. Based on the Taguchi method philosophy, the number of analysis configurations were reduced. It was desirable for the geometric characteristics of the aerobrakes chosen for analysis to represent the range of viable configurations. The entire design space was represented with nine configurations which consisted of permutations of three shapes and three diameter-to-depth ratios varying

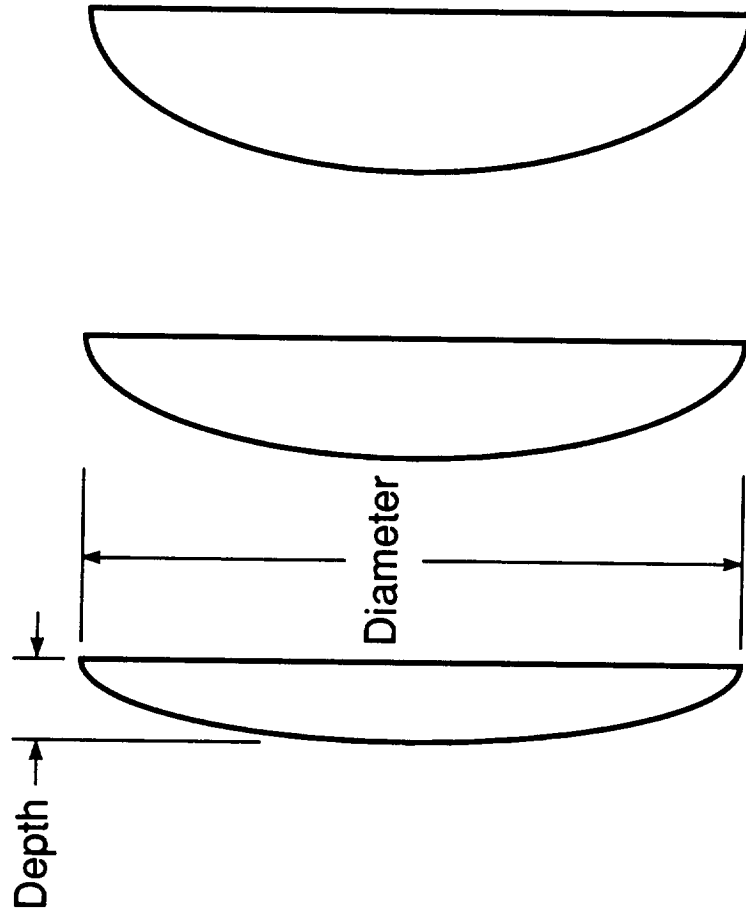
from four to six (Figs. 11-13). The three shapes are ellipsoid, spheroid, and sphere/cone. The ellipsoidal aerobrakes have an eccentricity of 0.5 (Fig. 11). The sphere/cone aerobrakes have an effective nose radius of 24 ft and a cone angle varying from 60 to 75 deg. (Fig. 12). The spheroidal aerobrakes have an effective nose radius varying from 32 to 64 ft. (Fig. 13).

The material selection as mentioned previously is based on projected technology availability. Three materials were chosen, each to represent a different level of technology. Aluminum was chosen to represent a state-of-the-art material. Aluminum-lithium was chosen to represent a near-term technology material. Carbon-carbon was selected to represent an advanced technology material.

Shape, diameter/depth, and material are aerodynamic, packaging, and technology parameters that impact the structural definition and weight of the aerobrake. The structural parameters include honeycomb thickness, number of radial frames, and number of ring frames. These parameters, among others, will dictate the structural integrity of the models.

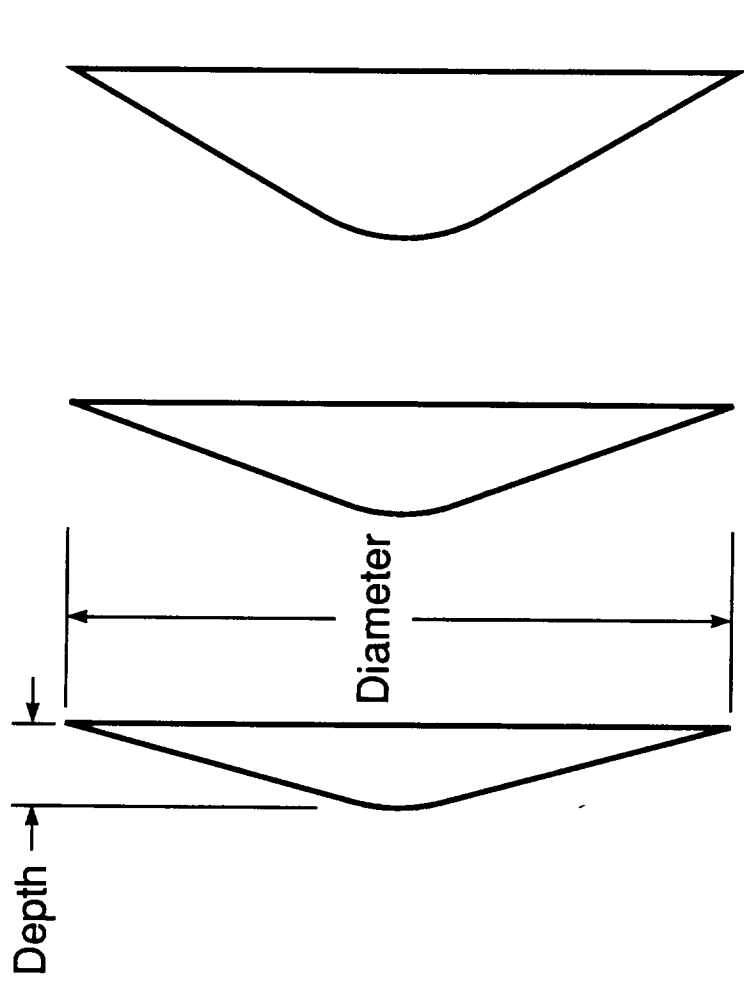
Based on the preliminary results the honeycomb thickness levels chosen were, 2.75, 3.0, and 3.25 inches.

The minimum number of radial frames was based on the number of payload-to-aerobrake attachment points which was chosen as five. To insure consistency across the finite element models, all are constructed with the same number of radial and circular surface elements. To increase the number of evenly distributed radial frames, while maintaining the five aerobrake to payload interfaces, the frames must be increased two-fold. The number of radial frames at level two are 10 and at level 3 are 20.



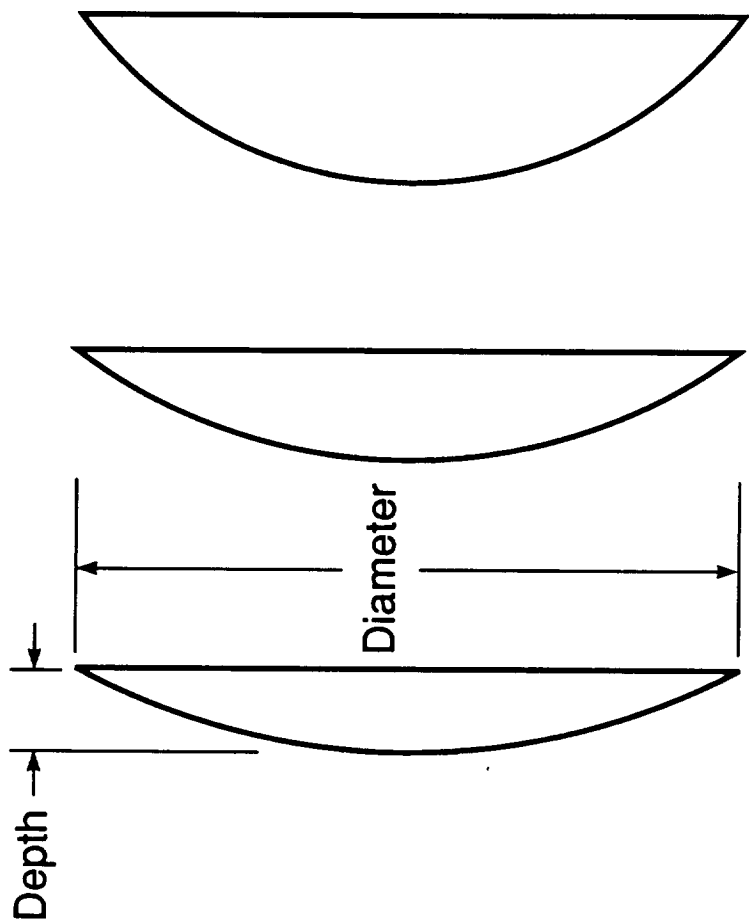
$\frac{\text{Diameter}}{\text{Depth}}$	8	6	4
Effective nose radius, ft	110	83	63

Figure 11. Ellipsoidal ($e = 0.5$) aerobrakes.



$\frac{\text{Diameter}}{\text{Depth}}$	8	6	4
Nose radius, R_N , ft	24	24	24
Cone angle, deg	75	70	60

Figure 12. Sphere/cone aerobreaks.



$\frac{\text{Diameter}}{\text{Depth}}$	8	6	4
Nose radius, ft	64	48	32

Figure 13. Spherical aerobreakes.

The number of concentric ring frames for testing are 4, 7, and 10. This range of values gives a sparse, medium, and dense distribution of concentric ring frames.

Many Taguchi matrices exist that can contain the six design parameters at three levels. Without studying the interactions, an L_{18} (18 experiments) matrix could be utilized. If one to three interactions are added, an L_{27} (27 experiments) matrix could be utilized. If more than three interactions are added, a larger matrix must be utilized. Three interactions were chosen, in an effort to reduce the amount of analysis time while maximizing the results. The three interactions involved all combinations of material, shape, and honeycomb thickness.

Given the six design parameters, their three interactions and three levels, a L_{27} Taguchi matrix was selected (Table I), and only 12 of 13 possible columns were needed. Each column represents a parameter or an interaction. The arrangement of the parameters and their levels are represented generically by the letters and numbers. Table II shows the actual experiment matrix combinations (interactions not shown). Each row represents an experiment, i.e., one combination of parameter levels.

Test Parameters	Shape	Honeycomb		AXE		Material			Frames	Rings	AXD	Diam/depth	Results			
	Col.	1	2	3	4	5	6	7	8	9	10	11	13	Aerobrake Weight	Aerobrake Weight +TPS	Global Buckling
No.		1	2	3	4	5	6	7	8	9	10	11	13			
1		1	1	1	1	1	1	1	1	1	1	1	1			
2		1	1	1	1	2	2	2	2	2	2	2	2			
3		1	1	1	1	3	3	3	3	3	3	3	3			
4		1	2	2	2	1	1	1	2	2	2	3	3			
5		1	2	2	2	2	2	2	3	3	3	1	1			
6		1	2	2	2	3	3	3	1	1	1	2	2			
7		1	3	3	3	1	1	1	3	3	3	2	2			
8		1	3	3	3	2	2	2	1	1	1	3	3			
9		1	3	3	3	3	3	3	2	2	2	1	1			
10		2	1	2	3	1	2	3	1	2	3	1	3			
11		2	1	2	3	2	3	1	2	3	1	2	1			
12		2	1	2	3	3	1	2	3	1	2	3	2			
13		2	2	3	1	1	2	3	2	3	1	3	2			
14		2	2	3	1	2	3	1	3	1	2	1	3			
15		2	2	3	1	3	1	2	1	2	3	2	1			
16		2	3	1	2	1	2	3	3	1	2	2	1			
17		2	3	1	2	2	3	1	1	2	3	3	2			
18		2	3	1	2	3	1	2	2	3	1	1	3			
19		3	1	3	2	1	3	2	1	3	2	1	2			
20		3	1	3	2	2	1	3	2	1	3	2	3			
21		3	1	3	2	3	2	1	3	2	1	3	1			
22		3	2	1	3	1	3	2	2	1	3	3	1			
23		3	2	1	3	2	1	3	3	2	1	1	2			
24		3	2	1	3	3	2	1	1	3	2	2	3			
25		3	3	2	1	1	3	2	3	2	1	2	3			
26		3	3	2	1	2	1	3	1	3	2	3	1			
27		3	3	2	1	3	2	1	2	1	3	1	2			

Table I. L₂₇ Taguchi matrix.

Test Parameters		Shape	Honeycomb	Material	Frames	Rings	Diam/depth	Results		
No.	Col.	1	2	5	9	10	13	Aerobrake Weight	Aerobrake Weight +TPS	Global Buckling
	1		E	2.75	Al	5	4	4		
2		E	2.75	Al-Li	10	7	6			
3		E	2.75	C-C	20	10	8			
4		E	3.00	Al	10	7	8			
5		E	3.00	Al-Li	20	10	4			
6		E	3.00	C-C	5	4	6			
7		E	3.25	Al	20	10	6			
8		E	3.25	Al-Li	5	4	8			
9		E	3.25	C-C	10	7	4			
10		S	2.75	Al	10	10	8			
11		S	2.75	Al-Li	20	4	4			
12		S	2.75	C-C	5	7	6			
13		S	3.00	Al	20	4	6			
14		S	3.00	Al-Li	5	7	8			
15		S	3.00	C-C	10	10	4			
16		S	3.25	Al	5	7	4			
17		S	3.25	Al-Li	10	10	6			
18		S	3.25	C-C	20	4	8			
19		SC	2.75	Al	20	7	6			
20		SC	2.75	Al-Li	5	10	8			
21		SC	2.75	C-C	10	4	4			
22		SC	3.00	Al	5	10	4			
23		SC	3.00	Al-Li	10	4	6			
24		SC	3.00	C-C	20	7	8			
25		SC	3.25	Al	10	4	8			
26		SC	3.25	Al-Li	20	7	4			
27		SC	3.25	C-C	5	10	6			

Table II. Experiment matrix.

Chapter VI - Results

The analysis results of the 27 experiments are shown in Table III. Aerobrake weights vary from a maximum of 10,144 lb to a minimum of 4351 lb. The experiments include aerobrakes with aluminum, aluminum-lithium, and carbon-carbon structures. To compare fairly the weights of these various material concepts, a thermal protection system weight is added to the aluminum and aluminum-lithium concepts but not to the carbon-carbon since this material can tolerate extremely high temperatures and operates as a hot structure. The TPS weight is approximated as the product of the surface area and an average thermal protection unit weight .

The aerobrake weights then vary from a maximum of 11656 lb to a minimum of 5145 lb. Global buckling sensitivity values vary from 5.66 to 0.28. These weights and global buckling values are used to derive the effects of each parameter on these critical values. An average weight for all 27 configurations at level one for each of the selected parameters is calculated. This step is repeated for levels two and three of each parameter. These averages are listed in the response table (Table IV). The relative sensitivity of each parameter on the weight is determined by subtracting the smallest value from the largest value in each parameter column. Number of frames and material selection show the highest sensitivity, meaning that the greatest effect on weight is realized by varying these parameters.

Test Parameters		Shape	Honeycomb	Material	Frames	Rings	Diam/depth	Results		
No.	Col.	1	2	5	9	10	13	Aerobrake Weight	Aerobrake Weight +TPS	Global Buckling
1		E	2.75	Al	5	4	4	5110	9838	1.05
2		E	2.75	Al-Li	10	7	6	4690	8639	0.56
3		E	2.75	C-C	20	10	8	9173	9173	2.23
4		E	3.00	Al	10	7	8	5123	8866	0.42
5		E	3.00	Al-Li	20	10	4	6470	11198	0.82
6		E	3.00	C-C	5	4	6	7842	7842	5.41
7		E	3.25	Al	20	10	6	6147	10096	0.75
8		E	3.25	Al-Li	5	4	8	4463	11656	0.40
9		E	3.25	C-C	10	7	4	7913	7913	4.75
10		S	2.75	Al	10	10	8	5330	9241	0.85
11		S	2.75	Al-Li	20	4	4	4951	9274	0.54
12		S	2.75	C-C	5	7	6	5145	5145	2.48
13		S	3.00	Al	20	4	6	4955	8824	0.90
14		S	3.00	Al-Li	5	7	8	4756	8667	0.81
15		S	3.00	C-C	10	10	4	6927	6927	2.42
16		S	3.25	Al	5	7	4	5453	9775	0.63
17		S	3.25	Al-Li	10	10	6	5370	9239	1.12
18		S	3.25	C-C	20	4	8	10144	10144	5.66
19		SC	2.75	Al	20	7	6	5190	8921	0.44
20		SC	2.75	Al-Li	5	10	8	4472	8105	0.25
21		SC	2.75	C-C	10	4	4	7224	7224	2.58
22		SC	3.00	Al	5	10	4	5247	9258	0.55
23		SC	3.00	Al-Li	10	4	6	4351	8082	0.33
24		SC	3.00	C-C	20	7	8	9927	9927	1.97
25		SC	3.25	Al	10	4	8	4856	8489	0.28
26		SC	3.25	Al-Li	20	7	4	5509	9520	0.58
27		SC	3.25	C-C	5	10	6	8662	8662	2.57
								Mean weight	8913	

Table III. Experiment matrix with results.

Parameter	Weight, lb					
	Honeycomb	Frame	Ring	Material	Shape	Diam/depth
Level-1	8396	8772	9042	9257	9469	8992
Level-2	8844	8291	8597	9376	8582	8384
Level-3	9500	9676	9100	8107	8688	9363
Sensitivity	1104	1385	503	1269	887	979

Table IV. Response table.

The optimum level for the three non-interacting parameters (frames, rings, and diameter/depth) can be selected by choosing the level within that parameter column with the lowest value for weight. Frames, rings and diameter/depth give optimum results at level two. That is, 7 frames, 10 rings, and diameter/depth of 6. Too many rings or frames add unnecessary weight to the structure, while a small number of ring frames reduces the overall stiffness of the structure and allows for global buckling. The weight of the rings and frames exhibit a “bucket” trend when plotted versus design level (Fig. 14).

The diameter/depth parameter has two effects on weight. As the diameter/depth is reduced, the amount of surface area is reduced, thereby reducing weight. Additionally, as the diameter/depth parameter is reduced the effect of the loading is increased due to a flattened shape, tending to increase weight. The balance between these effects occurs when the diameter/depth is 6.

Interacting parameters require an alternate method of determining the optimum level. For the three parameters for which interactions were examined, honeycomb thickness, material, and shape (Fig. 15), the weight at parameter one, level one is plotted versus all the levels of parameter two. A line is constructed connecting these data points. This is repeated on the same graph for second and third level of parameter one. If these lines are non-parallel, interactions occur; and if the lines cross, strong interactions occur between the parameters at these values. These plots verify that the expected strong interactions do indeed exist.

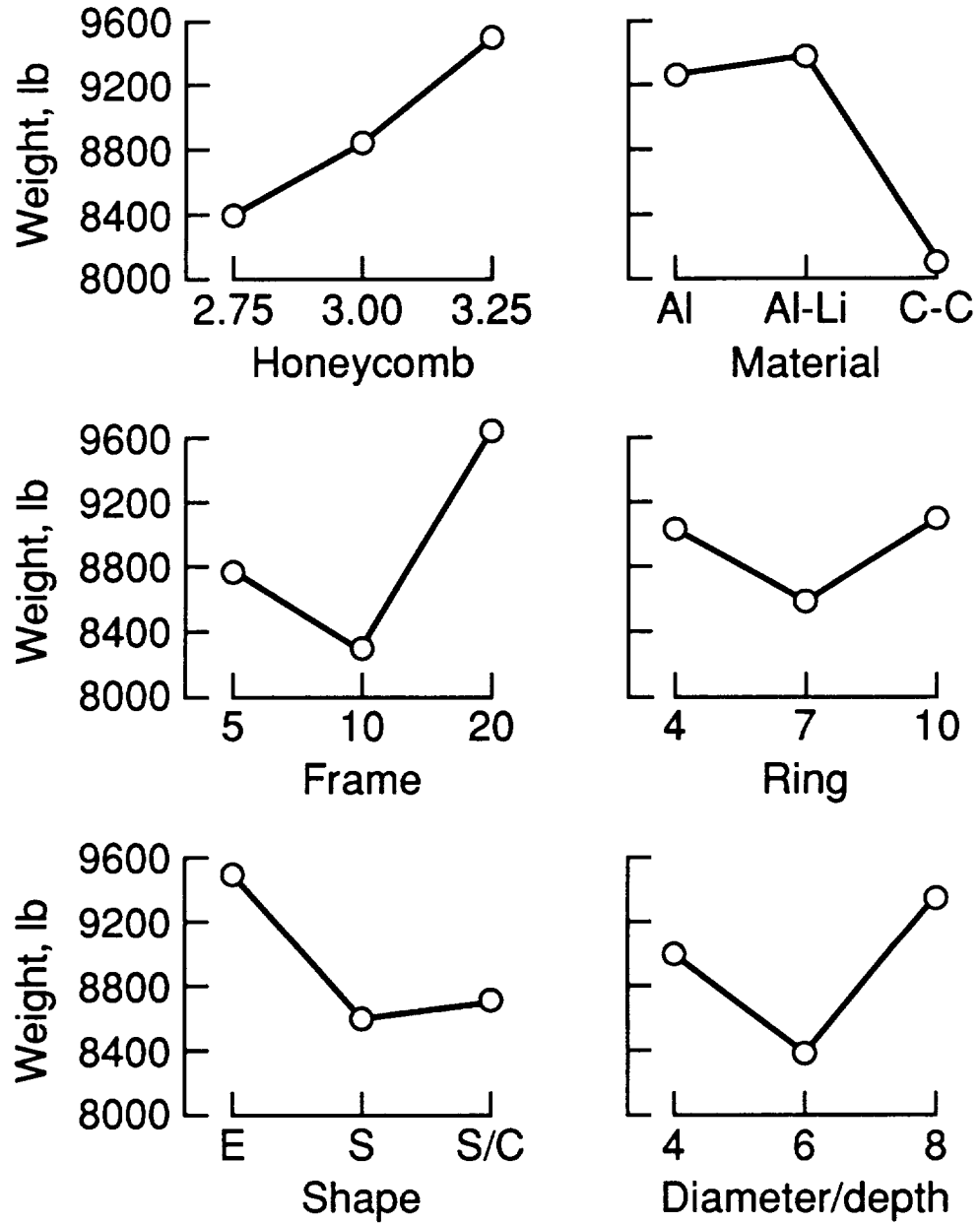


Figure 14. Response graphs.

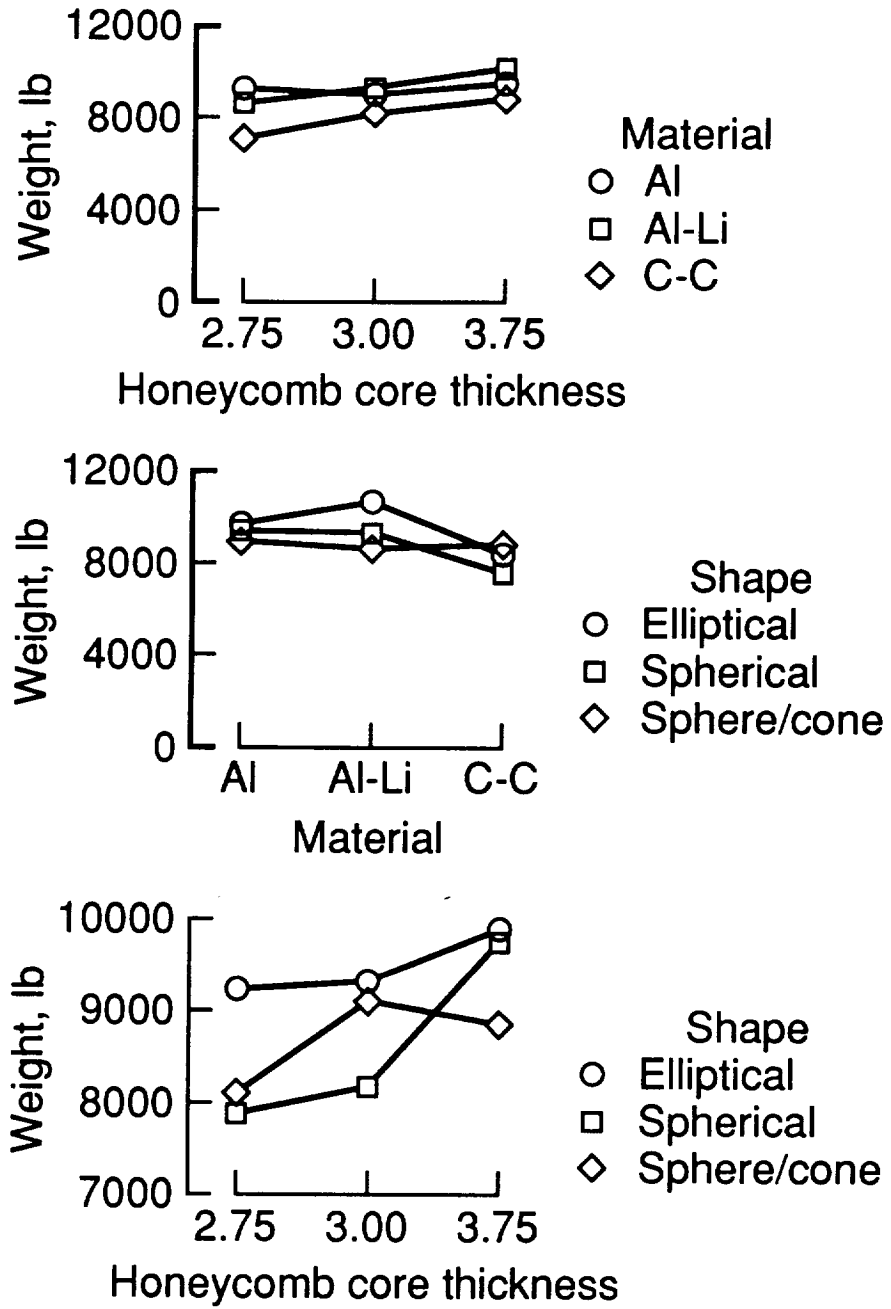


Figure 15. Interaction response graphs.

The parameter levels for the lowest weight combination for each graph are chosen as optimum levels. The honeycomb thickness-versus-material interaction graph displays an optimum combination of honeycomb thickness at level one (2.75 in) and a material level of three (carbon-carbon). The honeycomb thickness-versus-shape interaction graph displays an optimum combination of honeycomb thickness at level-1 (2.75 in) and a shape level of two (spheroid). The material-versus-shape interaction graph displays a optimum combination of material at level three (carbon-carbon) and a shape level of two (spheroid).

The optimum parameter levels for a minimum weight configuration of the aerobrake structure are circled in Table V. This combination of parameter levels represents the optimum combination within the prescribed design space. A review of the sensitivity plots for weight (Fig. 16) and global buckling (Fig. 17) shows that additional weight benefits may be realized by further reducing the honeycomb thickness. The honeycomb core thickness can only be reduced until the global buckling constraint of 1.0 is reached, where the aerobrake will globally buckle (Fig. 17). Therefore, the aerobrake was analyzed at four reduced honeycomb thicknesses while maintaining the optimum levels for the other parameters. The results are shown in Table VI. As the thickness of the honeycomb core thickness is reduced, the aerobrake weight is reduced and global buckling is being approached. A final honeycomb core thickness of 2.4 in. is selected because, at this honeycomb core thickness, the global buckling parameter is 2.13 and leaves a considerable margin of safety for global buckling. Thus, the optimum configuration yields a weight of 4971 lb, a 44 percent savings over the average weight of the experiment matrix cases.

	A	B	C	D	E	F
	Honeycomb	Frames	Rings	Material	Shape	Diam/depth
Level-1	2.75	5	4	Al	E	4
Level-2	3.00	10	7	Al-Li	S	6
Level-3	3.25	20	10	C-C	SC	8

Table V. Optimum configuration levels.

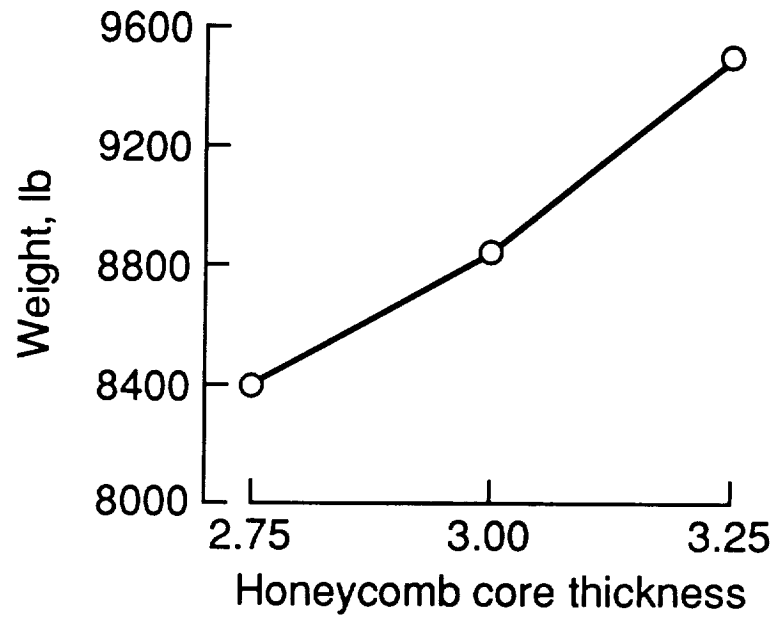


Figure 16. Weight sensitivity of honeycomb thickness.

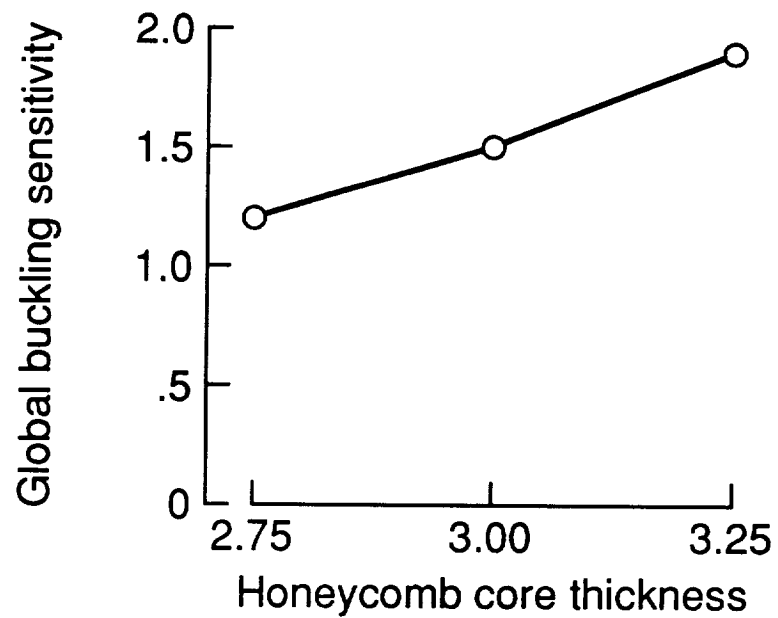


Figure 17. Global buckling sensitivity of honeycomb thickness.

Honeycomb thickness, in.	Weight, lb	Global buckling
2.6	5108	2.35
2.4	4971	2.13
2.2	4817	1.91
2.0	4653	1.70

Table VI. Honeycomb thickness optimization.

Chapter VII - Conclusions and Recommendations

The following conclusions are made based on the initial assumptions, input from other disciplines and the results of the design and analysis study.

The Taguchi design method and the finite element analysis method were successful in identifying, from among the design parameters tested, which ones have the most influence on the weight and global buckling. The aerobrake weight and global buckling are sensitive to all the parameters, but particularly to the honeycomb thickness, the number of radial frames, and the material.

Utilization of the Taguchi method significantly reduced the number of experimental configurations. Without the utilization of the Taguchi design method and the L_{27} orthogonal matrix, 729 experiments would have been necessary to find the lightest weight combination instead of the 27 in the study. The interactions and trends of the parameters could not have been captured without the use of the Taguchi method within the time constraints of the study.

The combination of Taguchi design method and the finite element analysis method appears to be an effective approach for conceptual/preliminary level aerobrake optimization studies. The average

aerobrake weight of all the experiments is 8913 lb, and the maximum weight is 11656 lb. The optimized structural weight of the aerobrake is 4971 lb., a weight savings of 3942 lbs over the average aerobrake weight.

Global buckling is a critical failure criteria for lunar aerobrakes. The preliminary study showed that while the aerobrake structure could be sized to withstand local failure criteria, the global buckling criteria could not always be satisfied.

The optimum level of the design parameters for minimizing weight are - 10 frames, 7 rings, 2.4 in honeycomb core thickness, carbon-carbon material, spheroidal shape, and a diameter-to-depth ratio of 6.

Interactions occur between the honeycomb thickness, the shape and the material. Changes in any of these parameters affect the impact of the remaining parameters.

Future lunar aerobrake structural design studies should include further considerations. Cost studies should be included since optimum weight configurations may not be synonymous with optimum cost. A thermal analysis of the aerobrake structure and its thermal protection system should be included to lend more detail to the weight estimations. Assembly and operational issues should be considered because they can have an impact on the weight and cost of the configuration.

List of References

1. Stafford, Thomas P., "America at the Threshold," May 1991
2. Braun, Robert D., "The Effect of Interplanetary Trajectory Options on a Manned Mars Aerobrake Configuration," M.S. Thesis, George Washington University, August, 1989.
3. "Lunar Aerobraked Vehicle Operations & Cost Assessment," Phase 3 Report, McDonnell Douglas Space Systems Company, July 1991.
4. "Lunar Aerobraked Vehicle Operations & Cost Assessment," Phase 2 Report, McDonnell Douglas Space Systems Company, April, 1991.
5. Rehder, John J., Cruz, Christopher I., Wurster, Kathryn E., Braun, Robert D., Bush, Lance B., "An Aerobrake Concept for Lunar Return," NASA TM, November, 1991.
6. Tippett, L. C. H., "Application of Statistical Methods to the Control of Quality in Industrial Production," Journal of Manchester Statistical Society, England 1934.
7. Taguchi, G., and Konishi, S., Taguchi Methods. Orthogonal arrays and Linear Graphs, American Suppliers Institute, Inc., 1987.
8. Sullivan, L.P., "The Power of Taguchi Methods," Quality Progress, June 1987, pp. 76-79.
9. Wille, R. H., "Landing Gear Weight Optimization Using Taguchi Analysis," SAWE Paper No. 1966, May 1990.
10. Advanced Materials & Processes, "1990 Guide to Selecting Engineering Materials," Volume 137, Issue 6, June 1990.
11. Russell, J. W., Trip report on visit to NASA Ames Research Center on April 9th and 10th, 1991, Lockheed, Engineering & Sciences Company, Hampton, Virginia, May 7, 1991.
12. Russell, J. W., Trip report on visit to Lockheed Missiles and Space Company on April 11th 1991, Lockheed, Engineering & Sciences Company, Hampton, Virginia, June 11th, 1991.
13. Phadke, S. M., Quality Engineering Using Robust Design, Prentice Hall, Englewood Cliffs, N.J., 1989.

14. Taguchi, G., Elsayed, E. and Hsiang, T., Quality Engineering in Production Systems, McGraw Hill, New York, N.Y., 1989..
15. American Supplier Institute Inc., "Taguchi Methods: Implementation Manual," ASI, Dearborn, MI, 1989.
16. McMillin, M. L.; Rehder, J. J.; Wilhite, A. W.; Schwing, J. L.; Spangler, J.; Mills, J. C., "A Solid Modeler for Aerospace Vehicle Preliminary Design," AIAA-87-2901, September 1987.
17. Bonner, E., Clever, W., and Dunn, K., "Aerodynamic Preliminary Analysis System II, Part I - Theory," 1989.
18. Sova, G., and Divan, P., "Aerodynamic Preliminary Analysis System II, Part II - User's Manual," 1989.
19. Brauer, G. L.; Cornick, D. E.; Olson, D. W.; Petersen, F. M.; and Stevenson, R., "Program to Optimize Simulated Trajectories (POST), Vol. II," MCR-87-583, NAS1-18147, September 1987.
20. Whetstone, W. D., "Engineering Analysis Language Reference Manual," Copyright 1983 by EISI, San Jose, CA, July 1983.
21. Cerro, Jeffrey A.; Shore C.P., "EZDESIT, A Computer Program for Structural Element Sizing and Vehicle Weight Prediction," NASA TM-101649, 1990.
22. Rourke, Raymond J., and Young, Warren C., Formulas for stress and strain, Fifth edition, McGraw-Hill Book Company, 1975.
23. "Military Standardization Handbook, Metallic Materials and Elements for Aerospace Vehicle Structures," MIL-HDBK-5B, July 1972.
24. "PATRAN Plus User's Manual," Release 2.5, Publication No. 219105, PDA Engineering, October, 1990.